JOURNAL OF APPLIED CRYSTALLOGRAPHY

Volume 49 (2016)

Supporting information for article:

On the forbidden and the optimum crystallographic variant of rutile in garnet

Shyh-Lung Hwang, Pouyan Shen, Hao-Tsu Chu and Tzen-Fu Yui

The samples and methods for TEM and EBSD data revisited in this paper

1. TEM

The UHP garnet samples for TEM study in Hwang *et al*. (2007; 2015) including two eclogitic samples (96Y5A/B) collected from the Yangkou layered mafic–ultramafic complex, Sulu UHP terrane and one diamondiferous quartzofeldspathic rock sample (25966) collected from Erzgebirge, Germany are revisited here. The eclogitic samples mainly consist of garnet porphyroblasts ($Prp_{29-41}Grs_{19-36}Alm_{33-45}Sps_{1}$) in a matrix of omphacite/clinopyroxene, fine-grained garnet and rutile (Zhang *et al*., 2005). The peak *P* – *T* condition was estimated to be 825 – 880°C and 42 – 45 kbar (Zhang *et al*., 2005). The porphyroblastic garnet is weakly zoned in almandine and grossular components, and contains abundant rutile needles up to 500 μm in length. Whereas the majority of rutile needles are along the $<111>_{grt}$ directions (see Fig. 1 in Hwang *et al*., 2007), minor $<100>_{grt}$ oriented needles are also present (see Fig. 11 in Hwang *et al*., 2015). The diamondiferous quartzofeldspathic sample consists of coarse-grained garnet crystals ($Prp_{28-39}Grs_{8-10}Alm_{53-65}$) in a matrix of quartz, phengite, biotite, kyanite, albitic plagioclase, K-feldspar, zircon, rutile and graphite (see Fig. 1 in Hwang *et al*., 2007). Abundant microdiamonds were found as inclusions in garnet (Hwang *et al*., 2006). The peak *P–T* condition was estimated to be 1200°C and >70 kbar (Massonne, 2003). Oriented rutile needles predominantly along $<111>_{grt}$ and subordinately along $<001>_{grt}$ directions are unevenly distributed in some garnet crystals (see Fig. 1 in Hwang *et al*., 2007 & Fig. 11 in Hwang *et al*., 2015).

The 4-ray and 6-ray Idaho star garnet samples in Hwang *et al*. (2015) as also re-examined here are derived from the schist/phyllite of the Wallace Formation, which is a mixed carbonate-siliciclastic sequence formed in a shallow-water environment and belongs to the Middle Proterozoic Belt Supergroup in western North America (Hietanen, 1968). (Please refers to Hwang *et al*. (2015) and references therein for the geological backgrounds.) The microstructure of 4-ray star garnet ($Prp_{11-13}Grs_{2-6}Alm_{81-84}Sps_{1-4}$) mainly consists of cloudy, red/brown "patches" of high abundance of rutile needles that are usually in coincidence with the ilmenite inclusion-rich domains in garnet cores (see Fig. 2 in Hwang *et al*., 2015). Within such "patches" the rutile needles are evenly distributed, ~10-100 μm in length, and oriented as 4 variants along the $<111>_{grt}$ directions (see Fig. 2 in Hwang *et al*., 2015). Many needles are in fact compound crystals comprising rutile and silica ± corundum ± kyanite ± aluminum hydroxide (Ti-akdalaite), based on SEM and TEM analyses (see Fig. 2 in Hwang *et al*., 2015). Abundant micrometer-sized zircon grains with cloudy cores, and submicrometer-sized facetted single or

multiple-phase inclusions consisting of zircon ± kyanite ± quartz ± brookite ± aluminum-hydroxide (Ti-akdalaite) are also omnipresent (see Fig. 2 in Hwang *et al*., 2015). The above rutile "patches" are separated by crystal clear domains, in which rutile needles, single or compound, occur exclusively within the linear, continuous, $<110>_{grt}$-oriented tube-like domains of <50 μm in diameter (see Fig. 2 in Hwang *et al*., 2015). Whereas rutile needles in 4-ray star garnet are exclusively oriented along the four $<111>_{grt}$ directions, the rutile needles in 6-ray star garnet are oriented along the four $<111>_{grt}$ and the three $<100>_{grt}$ directions and are concentrated within a thin $\{110\}_{grt}$ band of ~2–3 mm in thickness (see Figs. 1 & 3 in Hwang *et al*., 2015). Compared to 4-ray garnet, the 6-ray garnet has larger and longer rutile needles.

For TEM analysis, the thin sections of < 100 nm in thickness were either prepared by argon-ion-beam milling (Gatan PIS; operated at 4.0 kV, 9° incident angle; National Dong Hwa University), or were cut by FIB technique to specifically prepare end-on TEM thin sections having rutile needles nearly parallel to the sample surface (SMI 3050; National Sun Yat-sen University). Microstructures and compositions of minerals were studied using an analytical electron microscope (AEM, JEOL JEM-3010 operated at 300 kV; National Dong Hwa University) equipped with an energy dispersive X-ray (EDX) spectrometer (Oxford EDS-6636) with an ultra-thin window and a Si(Li) detector, capable of detecting elements from boron to uranium. TEM images and corresponding selected area electron diffraction (SAED) patterns were used to identify the crystallographic relationship between rutile needle and the garnet host. The precision of orientation determination from SAED pattern is better than 0.5°.

2. EBSD

EBSD samples studied by Proyer *et al*. (2013) are taken from a garnet–kyanite-bearing diamondiferous micaschist from the Kimi Complex of the Greek Rhodope massif (Proyer *et al*., 2013). This sample contains centimeter-sized garnets (~$Prp_{10}Grs_{15}Alm_{72}Sps_3$) embedded in a matrix of kyanite, biotite, muscovite, plagioclase, quartz and accessory minerals of rutile, apatite, zircon and monazite (Proyer *et al*., 2013). The estimated *P-T* conditions are 800 - 900°C and 12.7 - 16.3 kbar (Proyer *et al*., 2013). The garnets have poikilitic, diamond-bearing core surrounded by a clear rim, in which abundant rutile inclusions oriented in up to six directions were observed (see Fig. 1 in Proyer *et al*., 2013). The majority of such rutile inclusions have tiny cross-sections of 1- 2 μm (Proyer *et al*., 2013). The chemical analysis indicates a strong increase of Mg, a concomitant decrease in Fe, as well as the enrichment of trace

elements such as Mn, Y, P and Ti, but not Na, in the clear rim with rutile inclusions (see Fig. 1 in Proyer *et al*., 2013). Accessory minerals such as kyanite, apatite, quartz and zircon were also observed to be included in rutile-bearing domains. On the other hand, the metapegmatite sample studied by Griffiths *et al.* (2016) was collected from Wirtbartl, Austria. The Wirtbartl metapegmatites are intercalated with metapelites of the Austroalpine Saualpe-Koralpe crystalline basement complex (Schmid *et al*. 2004). The complex consists of poly-metamorphic siliciclastic metasediments with minor amphibolites, metapegmatites, and eclogites, as well as rare calc-silicates and marbles (Griffiths *et al.*, 2016). The EBSD sample consists of polycrystalline quartz ribbons, recrystallized feldspar and acicular kyanite defining a mylonitic foliation, as well as porphyroclastic magmatic garnet ($Prp_{1-3}Grs_{0-2}Alm_{52-59}Sps_{38-47}$) and K-feldspar of up to 1 cm in diameter (Griffiths *et al.*, 2016). Accessory minerals include tourmaline, apatite and zircon (Griffiths *et al.*, 2016). The estimated *P-T* conditions are 600-650°C and 4-6.5 kbar (Thöni *et al*. 2008; Griffiths *et al.*, 2016). The garnet core exhibits concentric and sector zoning defined by abundant submicrometer-sized inclusions, surrounded by clear rim intergrown with quartz and zircon (see Fig. 1 in Griffiths *et al.*, 2016). The inclusions defining the zoning are typically < 1 μm in diameter and include rutile, ilmenite, corundum, apatite, zircon, xenotime and qingheiite-Fe- (Griffiths *et al.*, 2016). Almost all inclusions that can be resolved optically are equant or slightly oblate, with no shape-preferred orientation (see Fig. 2 in Griffiths *et al.*, 2016). Rutile needles elongated along $<111>_{grt}$ are scarce.

The EBSD measurements in both Proyer *et al*. (2013) and Griffiths *et al.* (2016) were performed using FEI Quanta 3D FEG-SEM, equipped with an EDAX Digiview IV EBSD camera. The OIM Data Collection and EBSD analysis software packages were used for data processing. Analyses in Proyer *et al.* (2013) were performed at 20 kV accelerating voltage, 4 nA beam current, 1 mm aperture, 10 mm working distance and 20° beam incidence angle. A 2 × 2 binning of the EBSD camera resolution was applied, with Hough settings of 2° θ step size and a binned pattern size of 120 pixels. A 9 × 9 convolution mask was used for indexing 6–12 Hough peaks. The analyses in Griffiths *et al.* (2016) were performed at 15 kV accelerating voltage, 4 nA beam current, 14 mm working distance and 20° beam incidence angle. The EBSD camera binning was 2 × 2, with Hough settings of 1° θ step size and a binned pattern size of 140 pixels. A 9 × 9 convolution mask with a maximum of 16 bands was used for indexing garnet, and an 11 × 11 convolution mask with a maximum of 20 bands was used for indexing rutile. Whereas there is no estimation on the precision of orientation determination in Proyer *et al*. (2013), the estimated precision as determined between two independent measurements from the garnet matrix is ~1.4° in Griffiths *et al.* (2016).

Figure S1. The polar azimuthal equidistant projections of (a) $\{100\}_{rt}$ and (b) $\{001\}_{rt}$ poles of rutile in garnet from the UHP metapelites of the Kimi Complex (modified from Figs. 2c & 2f in Proyer *et al*. (2013)), showing the presence of minor COR-4 and R3b rutile (arrowed), as well as the $\{100\}_{rt}$ forbidden zones in the proximity of $<110>_{grt}$ poles (blue circles). Small open squares and circles in colors are garnet poles of specific hkl as denoted.

(a) (b)

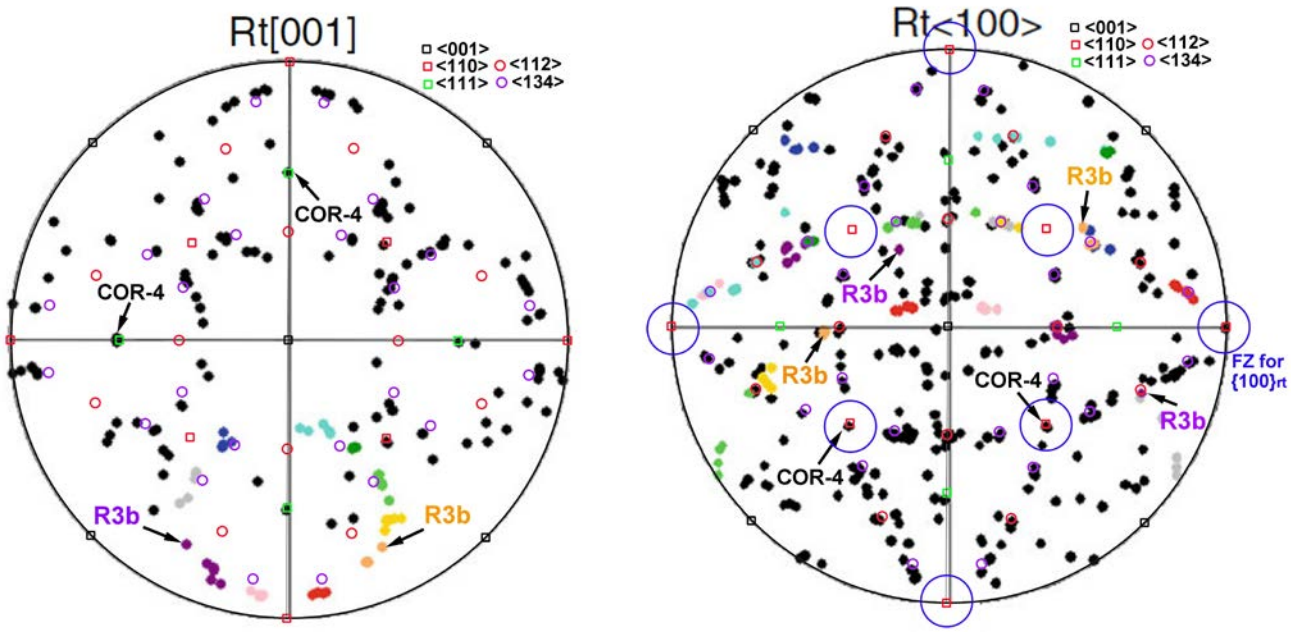

Figure S2. Projections of TiO_6 or MO_6 octahedra of rutile and garnet along various directions.

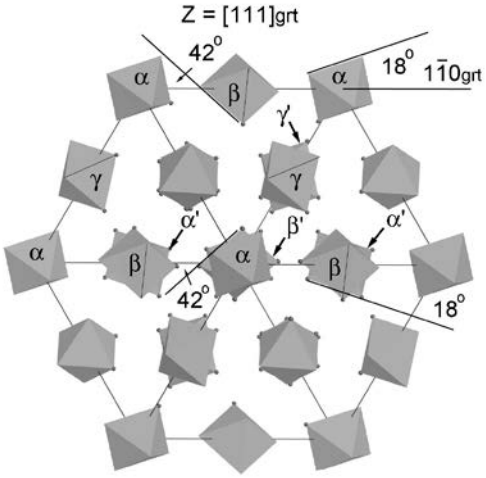

(a)

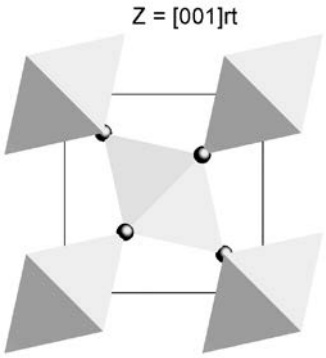

(b)

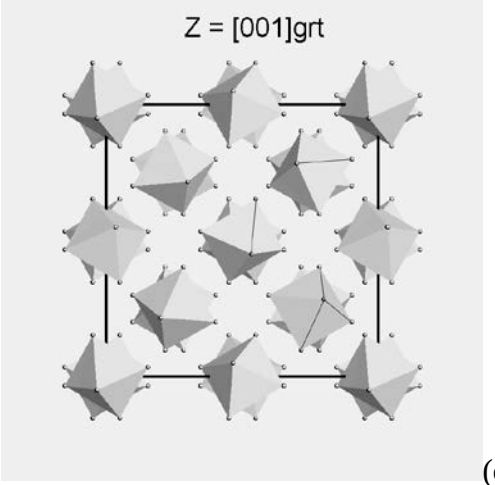

(c)

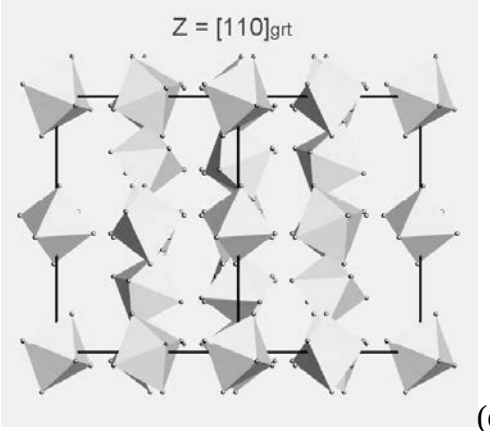

(d)

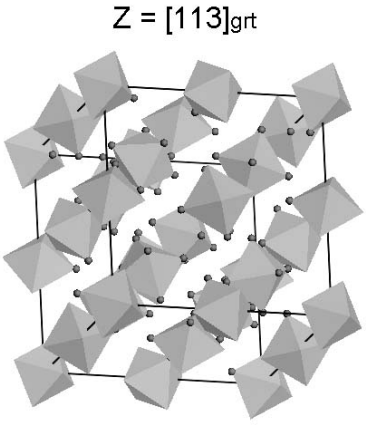

(e)

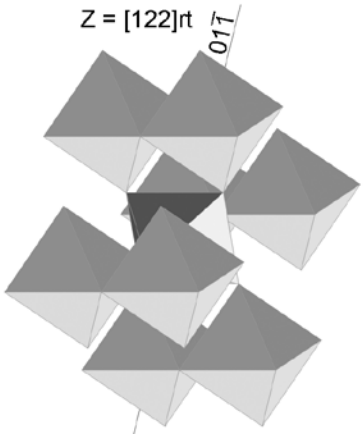

(f)